Mudbank dynamics: Field evidence of edge waves and far infra-gravity waves

R. Tatavarti, A. C. Narayana*, M. Ravishankar* and P. Manoj Kumar*

Naval Physical and Oceanographic Laboratory, Defence R&D Organization, Thrikkakara, Cochin 682 021, India
*Marine Geology Division, School of Marine Sciences, Cochin University of Science and Technology, Lake Side Campus, Fine Arts Avenue, Cochin 682 016, India

Field experiments in the nearshore ocean to understand the dynamics of *mudbank* off Kerala, south-west coast of India, are highlighted. Real time monitoring of the nearshore ocean off Purakkad, Kerala was made using pressure transducers for nearshore surface wave measurements, and current sensors for velocity measurements. Comprehensive information on the spatial structure of *mudbank* was obtained from aerial surveys (video recording from a helicopter). Extensive data collected on surface waves and currents in the nearshore ocean indicate that the infra-gravity (IG) waves (leaky modes and trapped edge wave modes) and far infra-gravity (FIG) waves, coupled with strong shoreline reflections and undertow, play an important role in the dynamics associated with the *mudbanks* off Kerala.

MUDBANKS are calm regions in the nearshore sea, devoid of any significant wave action due to high concentration of sediments in suspension. *Mudbanks* are unique and occur at only a few locations in the nearshore waters of the world oceans. Along the Indian coasts they are known to occur on the south-west coast especially off Purakkad in Kerala. The Kerala *mudbanks* were reported to generally appear with the onset of south-west monsoon—during May–June—and disappear with the withdrawal of the south-west monsoon. The *mudbank* appearing off Purakkad, Kerala has socio-economic implications as (i) it is known for its very high biological productivity[1–5], and (ii) it prevents the otherwise rampant sea erosion[6–8] during the south-west monsoon season along the Kerala coast.

Although numerous studies were made on the formation, sustenance and disappearance of the *mudbanks* off Kerala, the phenomenon still remains an enigma[9–14]. Once the *why* and *how* of these nearshore oceanic processes in terms of their occurrence and sustenance before disappearing are understood, the knowledge can be applied for preventing coastal erosion and for increasing the productivity of the nearshore oceans. We present here some of our findings based on the extensive field experiments (monitoring the nearshore waves and currents), and aerial surveys (video recording the entire coastal ocean in and around *mudbank*), to obtain a comprehensive picture of this phenomenon.

Infra-gravity edge waves

The dominant energy in the nearshore has long been considered to be composed of gravity waves and mean currents or circulation. The frequency bands of the gravity waves include the well-known wind wave and swell frequencies [$0(10^{-1})$ Hz] and the infra-gravity (IG) frequencies [$0(10^{-2})$ Hz]. The principal types of gravity wave motions that may contribute to the infra-gravity frequencies in the nearshore zone can be categorized into free waves and forced waves[15]. Free waves at the infra-gravity frequencies have been shown to consist of two types of surface gravity waves: alongshore progressive resonant edge wave modes trapped to the nearshore by refraction, and leaky wave modes that escape to deep water through reflection[16] and/or a second order surf zone generation mechanism due to wave breaking[17]. The trapped modes are topographically trapped to the shoreline (amplitudes exponentially decaying seawards) due to refraction and are called edge waves.

Edge waves are three dimensional in structure with an alongshore propagation, and with amplitudes largest at the shoreline. The theoretical prediction of the edge wave spectrum to be expected in the nearshore for given incident waves and topography is yet an unsolved problem[16]. Some of the theoretical problems that are hard to resolve are: (i) choice of the topographic smoothing scales both in the alongshore and cross-shore directions, (ii) modelling of the spatial forms of the different modes and the incompletely reflected waves, and (iii) the possibility of some forcing of surf beat within and outside the surf zone. Although it is difficult to distinguish between the leaky modes and trapped modes, the energy levels in the u (cross-shore) and v (alongshore) components of velocity measurements provide a *qualitative* indication of the presence or absence of edge waves[16,18]. The ratio of the energy in the v component to that of the u component of the velocity is larger (to the first order[18]) in the presence of edge waves than in the presence of near normal incidence leaky waves

alone. Moreover, it has been suggested that shoreline cusps are manifestations of sub-harmonic edge waves in the nearshore[19,20].

Far infra-gravity waves

Observations during the SUPERDUCK, USA experiment[21] revealed the presence of energetic alongshore progressive waves in 1 m water depth, with resolvable frequencies that typically fall into the lower end of the infra-gravity band. However, their alongshore wavenumbers were more than an order of magnitude larger than the alongshore wavenumber of mode 0 (zero) edge waves, suggesting that the motions were not of surface gravity waves. Recent investigations[22,23] demonstrated the existence of wave motions whose frequencies were typically in the range (10^{-3}–10^{-2} Hz), exceeding the traditional low frequency limit of the infra-gravity wave band. Hence these waves were called the far infra-gravity (FIG) waves[22]. FIG waves are a new class of nearshore waves based on the shear instability of a steady longshore current. The dynamics of FIG waves and surface gravity waves can be differentiated on the basis of their restoring mechanisms. While for surface gravity waves the restoring mechanism is gravity, for FIG waves it is the conservation of potential vorticity. It was suggested that the cross-shore shear structure of the mean longshore current supplies the background vorticity field. Perturbations of this field can be unstable, generating alongshore progressive, exponentially growing waves[22]. Oltman-Shay *et al.*[23] demonstrated the existence of a FIG frequency band that contains large amplitude, long period oscillations. The FIG waves have typical alongshore wavelengths and periods of the order of 10^2 m and s respectively, and can have rms velocity amplitudes greater than 30 cm/s. Furthermore, they were shown to occur only in the presence of mean longshore current and were unidirectional, changing celerity and direction with the mean longshore current magnitude and direction[23].

Field experiments, Mudbank-95

Field experiments were conducted in two phases in June and August 1995 by deploying pressure transducers (for monitoring wave elevations) and current meters (for monitoring nearshore ocean currents), off Purakkad, Kerala, in the nearshore waters of the Arabian Sea. Both pressure transducers and current meters were indigenously designed and fabricated. The pressure transducers were of stainless steel bellow type, while the current meters were bi-directional drag force sensors, designed to record the current speeds in any aligned direction (i.e. depending on the orientation of the current meter either the cross-shore component or the alongshore component of the nearshore velocity may be monitored). Sensor calibrations were performed in a towing tank with random wave generation facility. Extensive intercomparisons with other available standard instrumentation were made to assess the performance of the sensors. During the calibration and intercomparison experiments, checks for the robustness and sensitivity of the sensors were made. The response time of the pressure sensors and the current meters was found to be approximately 0.2 s. The frequency response of the pressure sensor was near unity between 0 and 2 Hz, while the frequency response of the current sensor was near unity between 0 and 5 Hz.

The sensors were deployed in the ocean by fixing them on stable underwater platforms, sitting on the ocean bed (Figure 1). Sensors (P_1, V_1) were collocated on a platform at a height of 1 m from the ocean bed, in 2 m water depth. Sensor pairs (P_2, U_2) and (P_3, U_3) were deployed in 5 m water depth, fixed on a platform. Sensors (P_2, U_2) were collocated at a height of 2 m from the ocean bed, while (P_3, U_3) were collocated at a height of 1 m from the ocean bed. The first platform in 2 m water depth was located at an offshore distance of 50 m from the shoreline, while the second platform in 5 m water depth was located at an offshore distance of 200 m from the shoreline. The sensor locations were so designed as to capture the horizontal and vertical structure of the nearshore wave and current regime. Underwater coaxial cables were used to transmit signals between sensors in the ocean and the shore-based control unit. Figure 2 shows a schematic representation of the real time data acquisition set up. The analogue signals from the control unit were piped through a A/D card (analogue to digital conversion) into a personal computer in order to store real time digital data. The frequency and duration of data sampling were controlled by the shore-based computer. Data were sampled at 2 Hz.

Aerial surveys of the *mudbank* and its surroundings

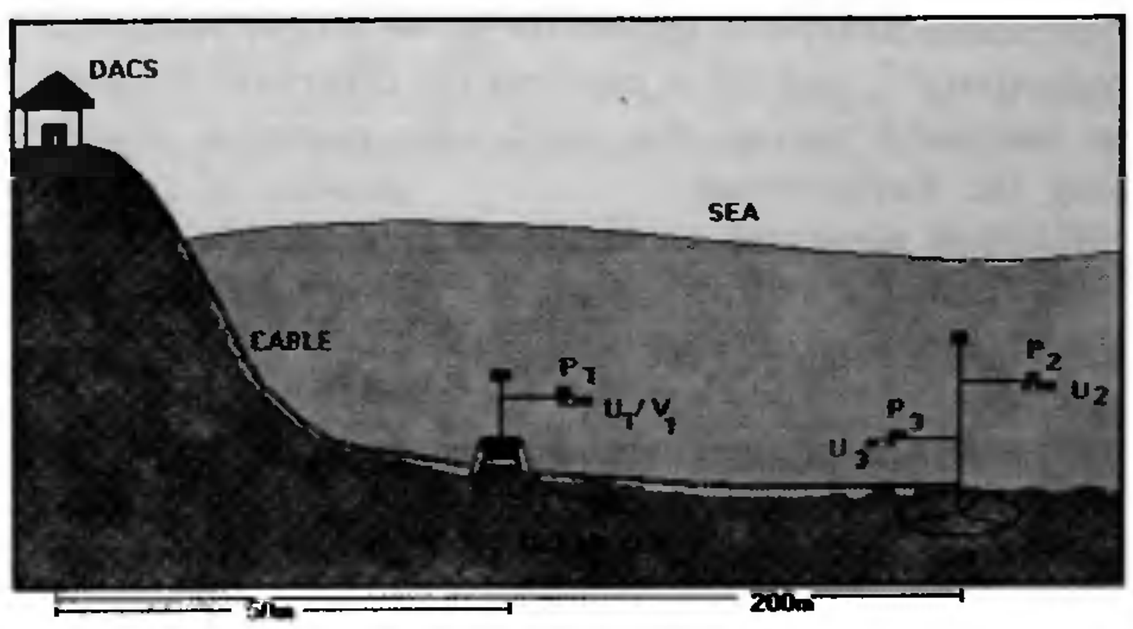

Figure 1. Section view of the sensor deployment on under-water platforms for data acquisition.

were conducted during the last week of June 1995 from a helicopter, to obtain a comprehensive picture in the spatial domain. The aerial survey coincided with our field experiments in the sea. Video recording was carried out using a CCD camera (Sony Betacam, Japan), on board the helicopter. Position fixing on board the helicopter, during aerial surveys and on a small vessel during bathymetry survey, was accomplished by using a portable Global Positioning System (Trimble GPS, USA) whose accuracy was ± 15 m. Bathymetry surveys were conducted using an echo sounder (Furuno, Japan).

Observations

Based on the recorded footage the schematic picture of the *mudbank* and its peripheries was drawn (Figure 3). The periphery of the *mudbank* extends to about 10 km seawards from the shoreline and stretches for about 15 km alongshore. The calm region is observed to be separated from the rough sea (significant wave height, $H_s \simeq 2.5$ m) by a transition zone where low frequency infra-gravity waves were observed (visually) to be dominant. The sediment concentration levels were the highest in the calm zone decreasing progressively towards the rough sea. The calm zone was observed to be buffeted by a straight shoreline, while the transition zone by shoreline cusps (Figure 3). During our observations we noticed a waxing and waning of the *mudbank* region with the changing wind conditions.

Strong onshore winds were responsible for the contraction of the *mudbank* region. At the northern and southern (shore normal) boundaries of the *mudbank* slowly propagating solitary waves were observed all the time. The *mudbank* region and its surrounding sea had significantly strong shoreline reflections of waves. Surging and spilling breakers were observed in the transition zone, while plunging breakers were observed in the rough zone. The surf zone in the transition zone inside the *mudbank* was narrow ($\simeq 10$ m), while that in the rough sea was wide ($\simeq 50$ m). During our daily inspection of sensors at low tides, we have felt very strong alongshore and cross-shore currents with a relatively long periodicity (low frequency). The sea bed was observed to have sinusoidal undulations (with vertical amplitudes of 5–10 cm and horizontal spacing of 1–2 m), slightly oblique to the shoreline. The beach cusp spacing in the transition zone, where our instruments were deployed, varied from 8.5 m to 26.5 m with average vertical amplitudes of 0.5 m.

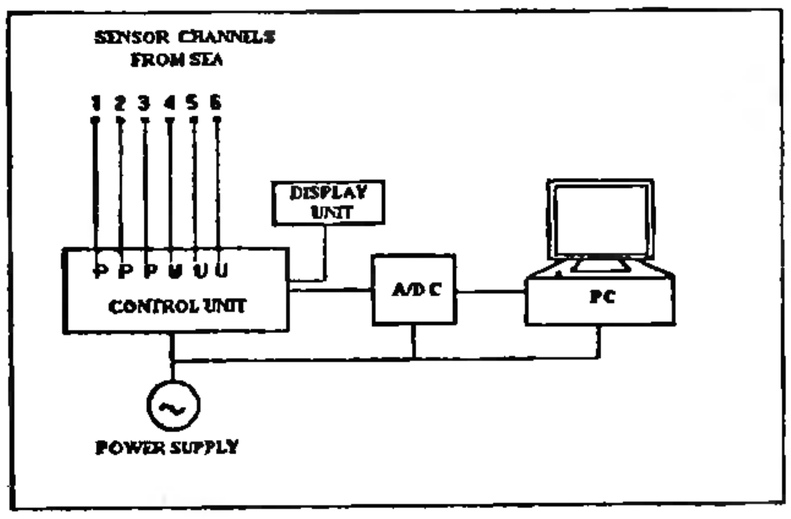

Figure 2. Schematic of real time data acquisition setup.

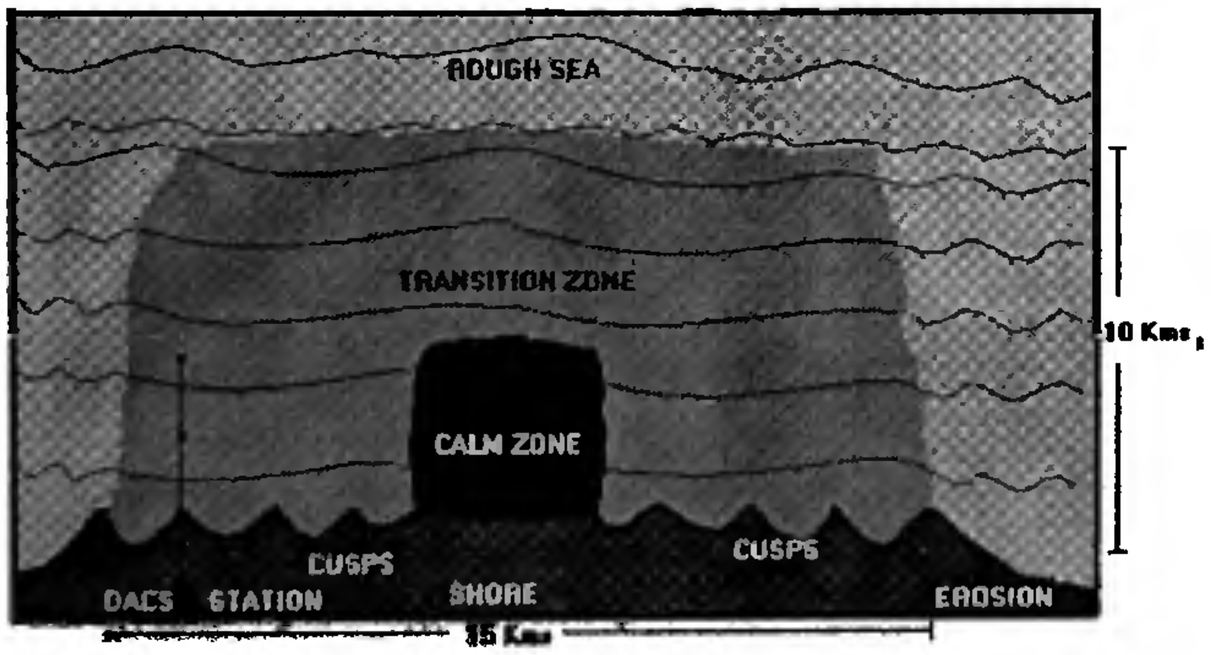

Figure 3. Schematic view of *mudbank* off Purakkad, Kerala, based on aerial survey.

Data for analysis

Although extensive data collection was carried out during the two phases (at 2 Hz sampling, for 5 and 10 day durations) of the field experiment, only representative data sets from the first phase of our experiments (specifically data recorded on the night of 24 June 1995 during low tide) are presented here to demonstrate the importance of infra-gravity and far infra-gravity wave bands in the dynamics of *mudbanks*. The following study is not purported to be exhaustive. The primary reasons for choosing this specific data set were that (i) on 24 June 1995, strong alongshore currents towards north were noticed during our periodic inspection of sensors, and (ii) a very long data set (9 h duration) was recorded on that night during which time the tide was ebbing.

Results and discussion

Care was taken while analysing the data sets, not to contaminate the analysis with any existing trends in time series (for instance, mean longshore current and tidal trends). The spectra shown in this paper were generated from consecutive 4096 s time series sections. Each section was detrended using a quadratic function (to remove tide) and demeaned before Fourier transformation. Typical sections of 25 min long raw time series

of the alongshore component (v) from V_1, cross-shore component (u) from U_3 and the surface elevation [$p(\eta)$] from P_1 are presented in Figure 4. Sensors V_1 and P_1 are collocated, while sensor U_3 is located 150 m seawards of P_1, V_1 sensor pair (see Figure 1). For this particular data set, as cross-shore currents were not monitored along with the collocated observations of η and v from P_1, V_1 sensors respectively, we present the cross-shore current (u) from the U_3 sensor at the 5 m water depth location, as an alternative for comparison. As can be seen there are no trends and offsets in the time series to contaminate our spectral computations. Large amplitudes (~ 0.2 m/s), and long period oscillations (100 to 1000 s) are present in the alongshore component of the velocity (Figure 4 *a*). Cross-shore velocity U_3 at a location of 150 m seawards of the alongshore velocity sensor (Figure 4 *b*) also shows these oscillations but they are less pronounced. Oscillations with periodicities of approximately 40 and 500 s are prominent in the surface elevation time series record from the sensor P_1 collocated with the alongshore velocity sensor V_1 (Figure 4 *c*), the amplitudes of the longer periods having larger amplitudes. The variance associated with these oscillations is evident in the frequency spectra (Figures 5 and 6).

Spectral computations were made using a 50% overlap Hanning spectral window having 60 degrees of freedom (dof) and a frequency resolution of 0.00048 Hz. Typical spectra of wave elevation (η) from P_1 sensor, cross-shore current (u) from U_3 sensor, and alongshore current (v) from V_1 sensor are shown in Figure 5. Spectra of data monitored at 2140 h on 24 June 1995 from P_1, U_3 sensors were compared with those obtained with data observed at 1410 h from P_1, U_1 sensors on the same day (Figure 6). This enabled us to make *qualitative* speculations about the cross-shore currents at the inshore location (water depth, 2 m) where significantly stronger alongshore velocity V_1 was observed from the 2140 h data set. Assuming that the u monitored at the 2 m water depth at 1410 h is statistically representative of u at the same location at 2140 h (i.e. assuming stationarity in the time series observations), we can infer from Figure 6 that the cross-shore velocity variance progres-

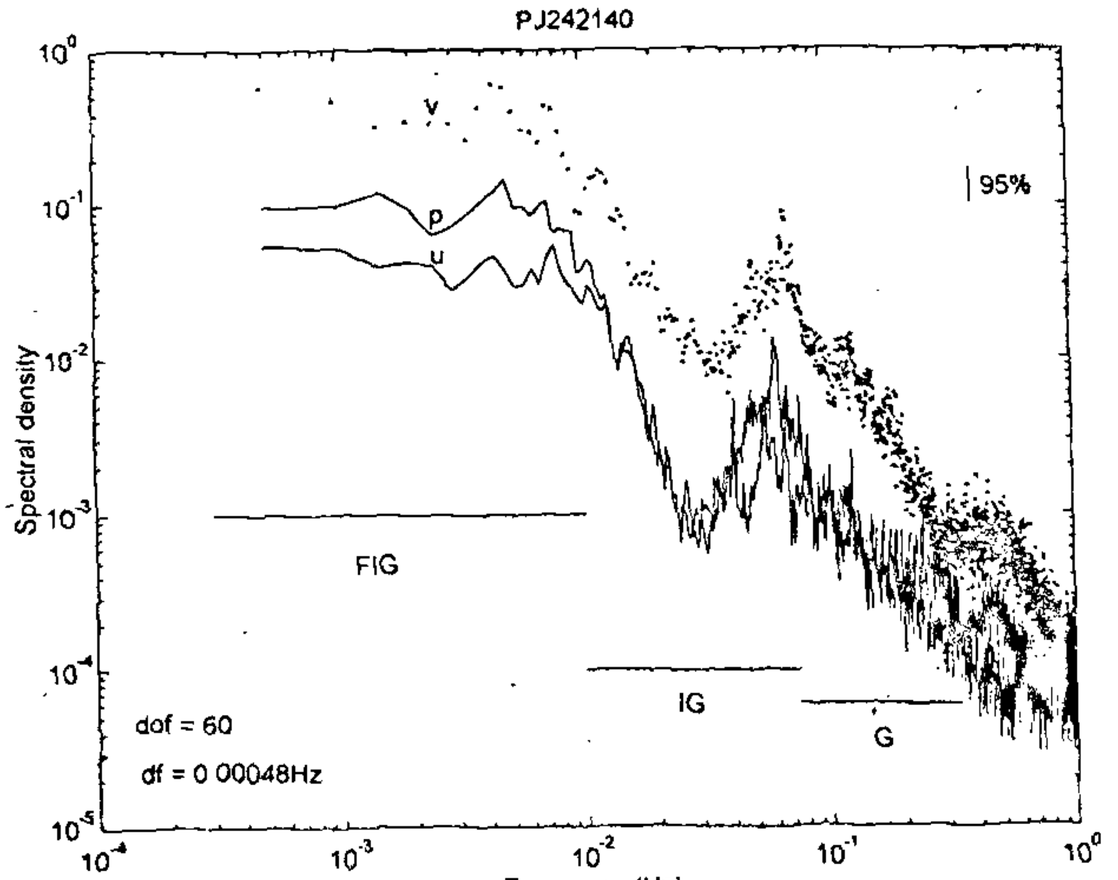

Figure 5. Spectra of v, u and $p(\eta)$. The FIG, IG and G bands are marked. Data from V_1, U_3 and P_1 sensors at 2140 h 95% confidence levels are shown in the upper right corner. DOF = 60, and frequency resolution is 0.000488 Hz.

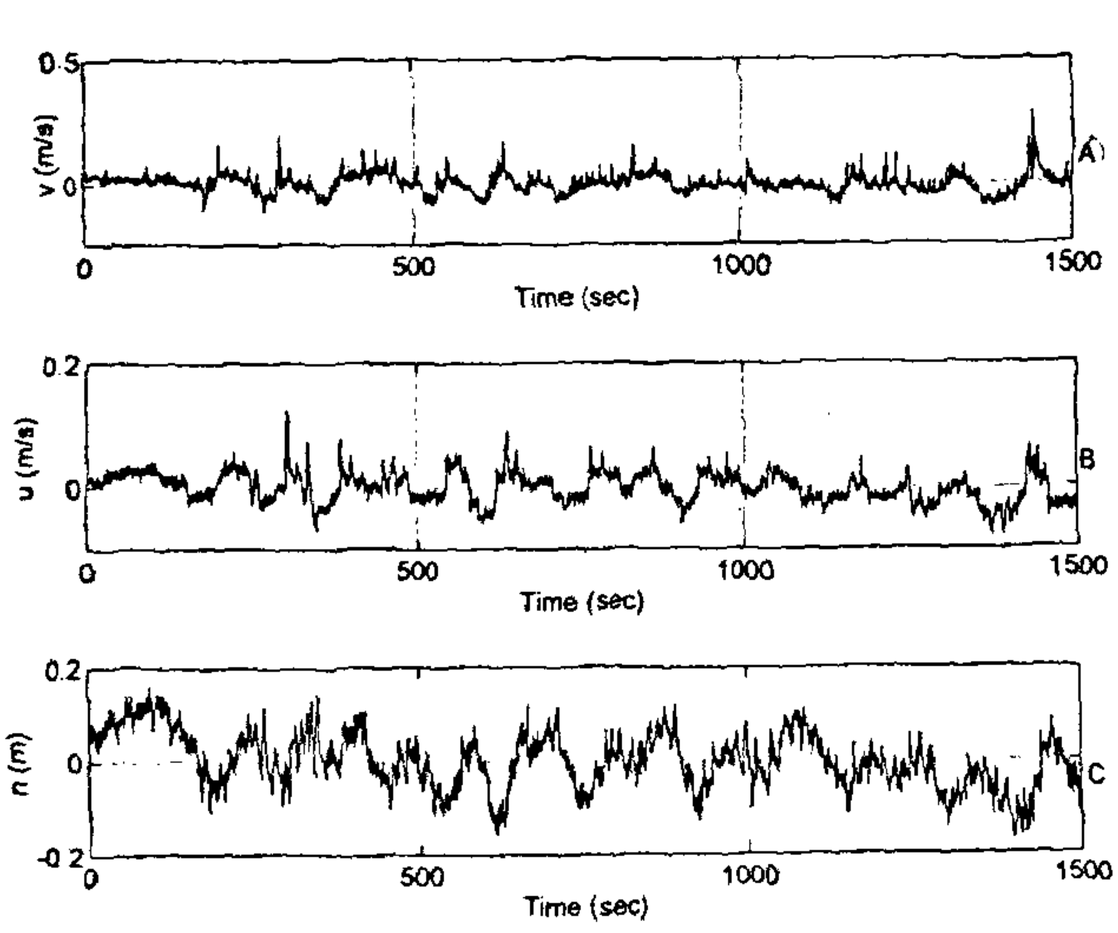

Figure 4. Representative time series of v, u and η from the data set collected on 24 June 1995 at 2140 h during ebbing tide. The data were demeaned and detrended. Observations of v and η were from collocated sensors while u is from a sensor 150 m seawards.

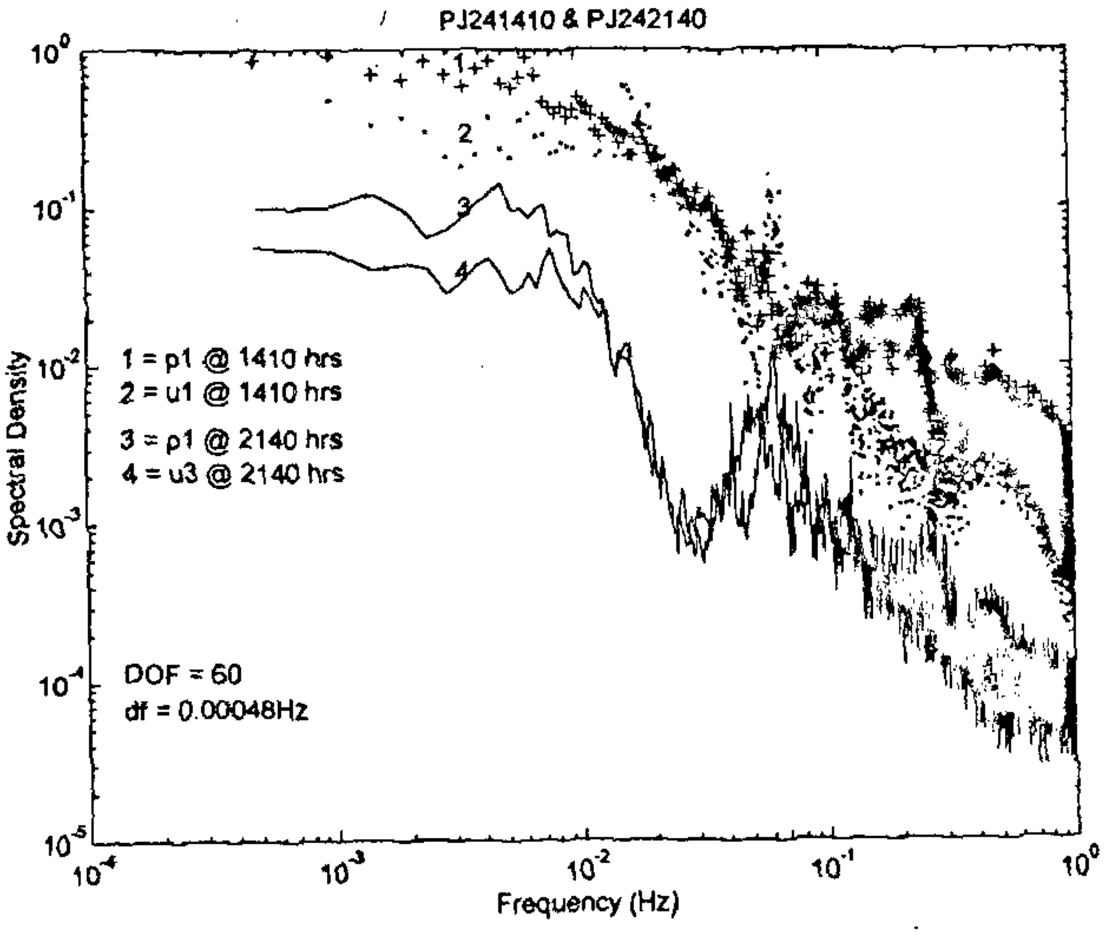

Figure 6. Spectra of data from collocated sensors P_1 and U_1 corresponding to the observations at 1410 h (1 and 2) and spectra of data from sensors P_1 and U_3 corresponding to observations at 2140 h (3 and 4). Statistics of spectra are the same as those of Figure 5.

sively increases as the waves approach the shore (consistent with the shoaling hypothesis). On the basis of observations from all the data sets we noticed that (i) the cross-shore currents increase in magnitude shorewards (i.e. from the 200 m seaward location to the 50 m seaward location with respect to the shore), (ii) the wave elevations decrease in magnitude shorewards, (iii) the ratio of the amplitude of alongshore current (v) to that of the cross-shore current (u) generally ranges from 0.5246 to 0.8745, and (iv) there was significant change in magnitudes of the nearshore alongshore velocity components (v) along the cross-shore direction denoting significant shear, which may be the reason for the presence of FIG wave motions. Figure 6 shows some of the features consistent with wave shoaling. The shoreward decreasing wave elevation (i.e. from 200 m offshore location to 50 m location) may be speculated to be the result of viscous damping due to the increase in suspended sediment concentrations in the water column. As no wave breaking is observed even at 50 m offshore location, it may be speculated that the energy lost from the waves is transferred to the currents in the region. This speculation explains the increase in the cross-shore currents at the 50 m offshore location. Spectra from V_1 and U_2, U_3 sensors based on measurements at water depths of 2 m and 5 m respectively are shown in Figure 7, while Figure 8 shows the spectra from P_1, P_2 and P_3 sensors. The 95% confidence levels are the same for all spectra and are shown along with the spectra only in Figure 5. Three features that stand out from Figures 5–8 are (i) the low frequency energies in all spectra are maximum, the FIG band (10^{-3}–10^{-2} Hz) of frequencies having about two orders of magnitude more energy compared to the gravity (G) band of frequencies (10^{-1} Hz); (ii) the ratio of the variance in the alongshore component (v) to that in the cross-shore component (u) of the nearshore velocity, is significantly higher, especially in the FIG and infra-gravity (IG) frequency bands; (iii) the wind wave frequency band (G-band) is least energetic. The features in the IG band of the spectra in Figures 5 and 6, i.e. $\langle v^2 \rangle \approx \langle u^2 \rangle$, along with our visual observations of shoreline cusps are consistent with edge wave dynamics (i.e. the presence of trapped modes in the IG frequency band). The fact that the ratio of variance in the v component to that of the variance in the u component is larger in the FIG band (Figures 5 and 6) suggests the role of a strong alongshore current and is consistent with FIG wave dynamics discussed earlier. The vertical and horizontal structure in the nearshore can also be noticed in Figures 5–8, as the sensors from different horizontal and vertical locations exhibit changing spectral features consistent with IG (leaky and trapped modes) and FIG waves. The larger FIG band variance in U_3 located closer to the ocean bed, compared to that in U_2 in Figure 7 is perhaps indicative of a strong undertow[24]. This speculation is further justified when observing the spectra from P_2, P_3 sensors in Figure 8, which are collocated with U_2, U_3 sensors respectively. The identical spectra of P_2 and P_3 in all frequency bands (Figure 8) coupled with identical spectra of U_2 and U_3 in all but the low-frequency bands, where the variance in U_3 is larger than that in U_2 (Figure 7), clearly suggests the presence of a strong undertow. The lower FIG band variance in P_1 relative to P_2 and P_3 is consistent with the suggestion of Oltman-Shay *et al.*[23], that FIG band variance may not show up in the surface displacement measurements. Phase and coherence between the horizontal velocity components

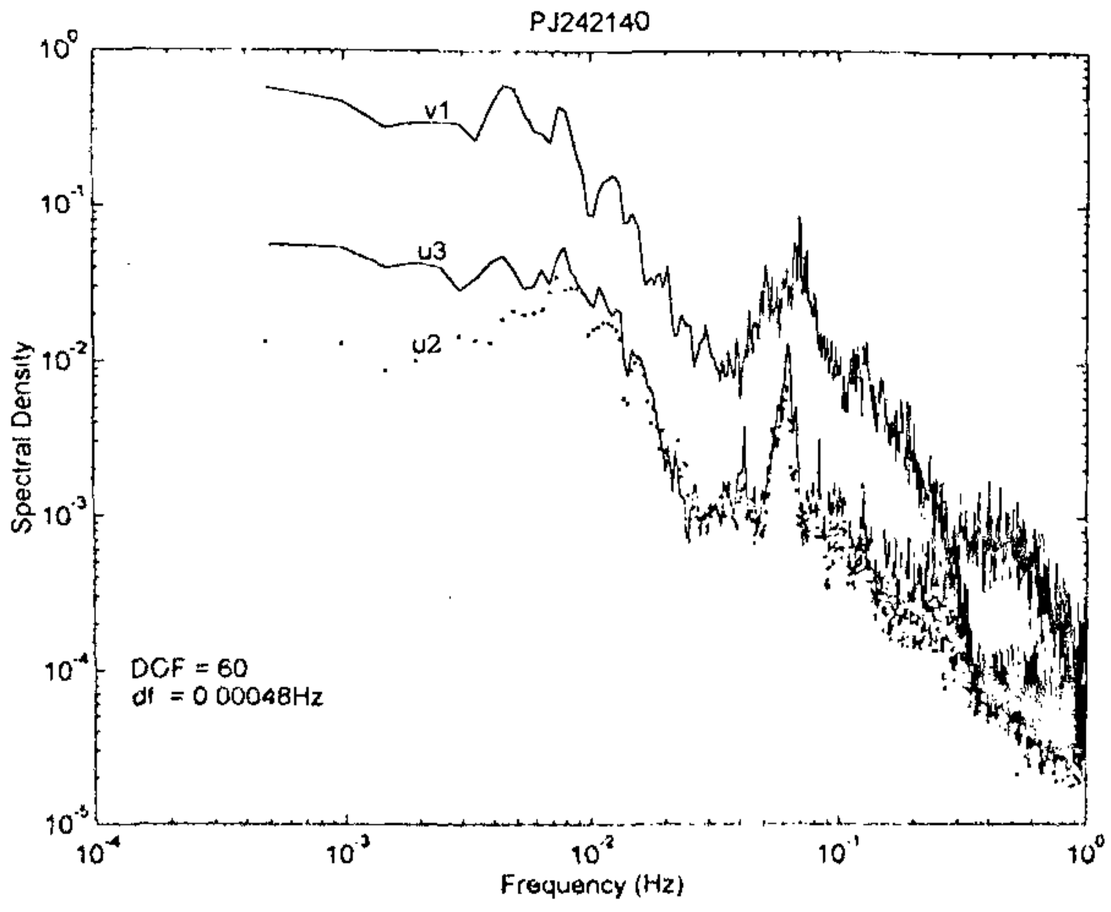

Figure 7. Spectra of data at 2140 h from sensors V_1, U_2 and U_3. Statistics of spectra are the same as those of Figure 5.

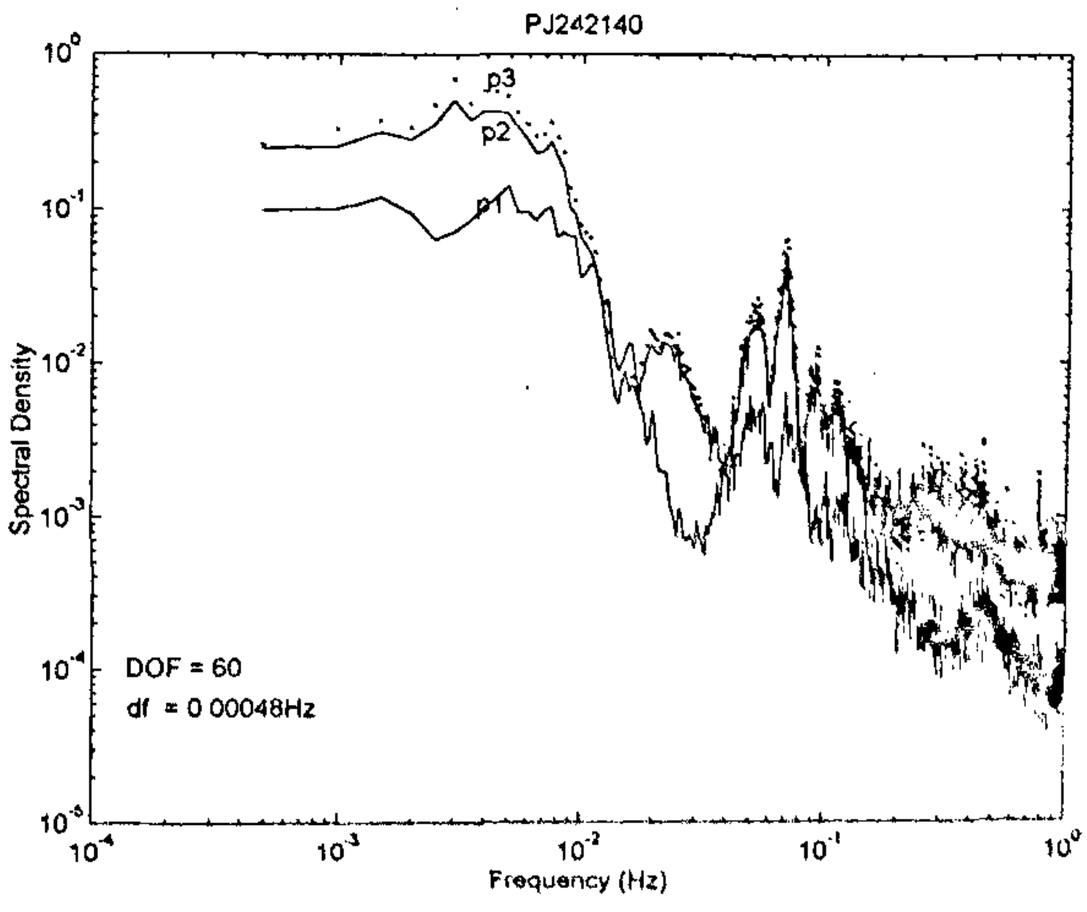

Figure 8. Spectra of data at 2140 h from sensors P_1, P_2 and P_3. Statistics of spectra are the same as those of Figure 5.

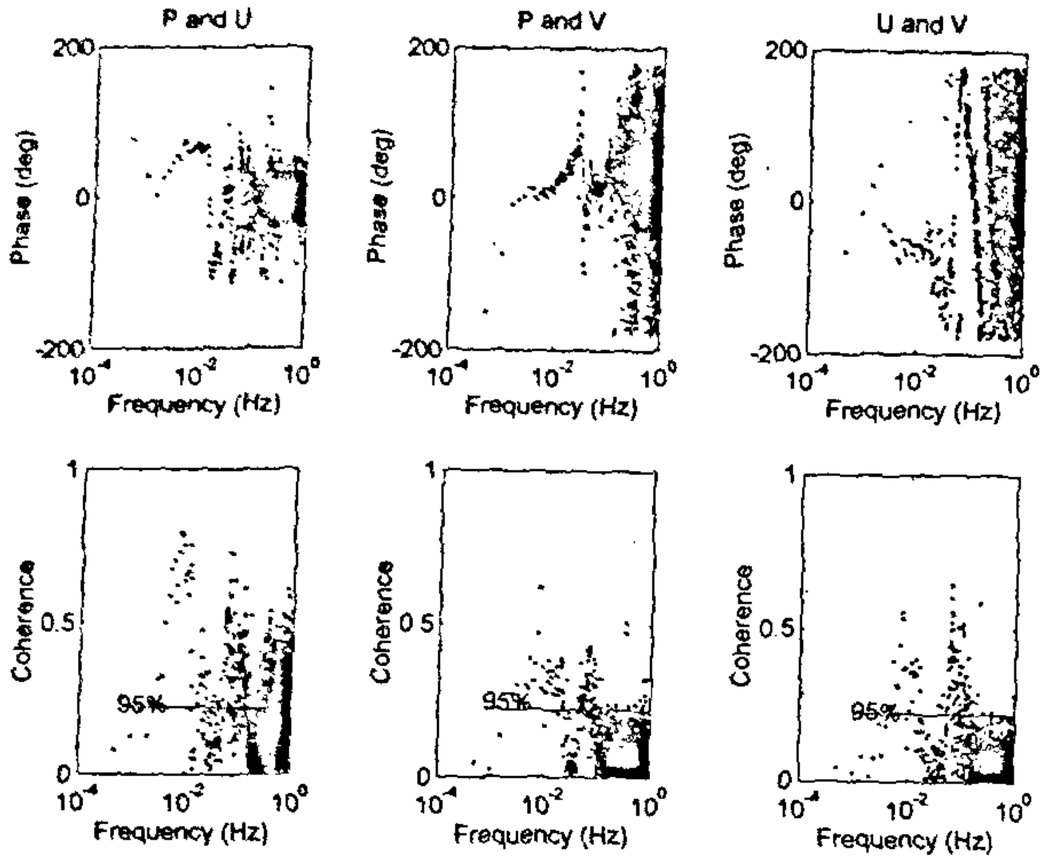

Figure 9. Cross-spectral phase and coherence plots for data from P_2U_2, P_1V_1 and U_2V_1 pairs of sensors. Statistics of spectra are the same as those in Figure 5. The 95% upper confidence level for coherence is drawn as a horizontal line in the coherence plots.

and the surface elevation are shown in Figure 9. The time series at 2140 h from (P_2, U_2), (P_1, V_1) and (U_2, V_1) sensor pairs were used for cross-spectral phase and coherence computations. The horizontal line in the coherence plots of Figure 9 denotes the upper 95% confidence level on coherence. Generally there is significant coherence in the FIG band between the velocity components and the surface elevation, with an in-phase relationship between P and V and out-of-phase relationship between P and U, and U and V measurements. The coherence in the IG band is also significant, but the coherence in the gravity wave band is not significant, except between P and U. In the FIG band the highest coherence is between P and U, with P leading U in quadrature. It is also found that in the FIG band P leads V in quadrature while V leads U in quadrature. These results are consistent with the characteristics of FIG waves[23]. In the IG band the highest coherence was found between P, U and U, V pairs of series although the coherence between P, V pair is also significant. It can be noticed from Figure 9, that in the IG band, P leads U and V in quadrature, while V leads U in phase. These features in the IG band are consistent with the standing edge wave dynamics[25]. The constant time lag associated with the linear phase (with frequency) in the gravity wave frequency band between V and U phases in Figure 9 is indicative of the travel time associated with the distance of separation ($\simeq 150$ m) between U_2 and V_1 sensors.

Naturally occurring frequency-dependent shoreline reflections were computed following the noise-free technique developed by Tatavarti[16] and validated by Huntley *et al.*[26], utilizing time series measurements from collocated η and u sensors. Details of computations are not being presented here as they do not easily fit into the scope of this short paper. Only the mean shoreline reflection coefficients are discussed. It was observed that generally the reflections in all frequency bands were significantly high (0.6), highest being in the lower frequencies (0.8). These strong reflections are consistent with our observations of sea bed undulations[27].

Conclusions

Extensive field experiments conducted in the *mudbank* off Purakkad, Kerala provided a comprehensive picture of the unique phenomenon. Based on the analysis of a typical data set collected at a sampling rate of 2 Hz, for a duration of 9 h, the following conclusions are drawn. Our analysis established that far infra-gravity (FIG) wave energy is about two orders of magnitude larger than that of gravity waves. Evidence of edge waves in the infra-gravity band was demonstrated. This is presumably the first study to establish the evidence of FIG and edge waves in the *mudbank* region. The demonstration of FIG waves supports the suggestion of Bowen and Holman[22], that FIG waves may be a common feature in the nearshore oceans in the presence of longshore currents.

The computed shoreline reflections were observed to be very high, with approximately 80% of the low-frequency waves being reflective. Even gravity waves were found to be strongly reflective (mean reflection coefficient of 0.6). Our data analyses also demonstrated the presence of a strong undertow. The predominant low-frequency wave energy and associated reflections, coupled with a strong undertow, question the validity of constructing seawalls for prevention of coastal erosion[28,29] along the Kerala coast.

We conclude that the infra-gravity waves (trapped edge modes and leaky modes), FIG waves and undertow play an important role in *mudbank* dynamics and need to be considered in the modelling of *mudbanks*.

1. Gopinathan, C. P. and Quasim, S. Z., *Indian J. Mar. Sci.*, 1974, **3**, 105–114.
2. Damodaran, R., *Bull. Dept. Mar. Sci.*, 1973, **VI**, 1–126.
3. Nair, P. V. R. *et al.*, *CMFRI Bull.*, 1984, **31**, 28–34.
4. Rao, D. S. *et al.*, *CMFRI Bull.*, 1984, **31**, 25–27.
5. Thompson, P. K. R., *J. Mar. Biol. Assoc.*, 1986, **28**, 48–56.
6. Kurup, P. G., *Bull. Dept. Mar. Sci.*, 1977, **VIII**, 1–72.
7. Nair, A. S. K., Proceedings of the Coastal & Ocean Engineering Conference, 1985, vol. 2, pp. 468–479.
8. Silas, E. G., *CMFRI Bull.*, 1984, **31**, 2–7.
9. Nair, R. R., *Am. Assoc. Pet. Geol.*, 1976, **64**, 616–621.
10. Froidefond, J. M., Pujos, M. and Andre, X., *J. Mar. Geol.*, 1988, **84**, 19–30.
11. Faas, R. W., *EOS Trans. AGU*, 1992, **73**, 290.
12. Faas, R. W., *Geo Mar. Lett.*, 1991, **11**, 143–146.

13. Mehta, A. J. and Jiang, Tech. Rep. Coastal and Ocean Engg. Dept., Univ. of Florida, 1993.
14. Wells, J. T. and Coleman, J. M., *J. Sed. Petrol.*, 1981, **51**, 1069–1075.
15. Bowen, A. J. and Huntley, D. A., *Mar. Geol.*, 1984, **60**, 1–13.
16. Tatavarti V. S. N. Rao, Ph D thesis, Dalhousie Univ., Canada, 1989, pp. 175.
17. Symonds, G., Huntley, D. A. and Bowen, A. J., *J. Geophys. Res.*, 1982, **87**, 492–498.
18. Huntley, D. A., *J. Geophys. Res.*, 1976, **81**, 6441–6449.
19. Bowen, A. J. and Guza, R. T., *J. Geophys. Res.*, 1978, **83**, 1913–1920.
20. Holman, R. A. and Bowen, A. J., *J. Geophys. Res.*, 1982, **87**, 457–468.
21. Crowson, R. A., Birkemeir, W. A., Klein, H. M. and Miller, H. C., Tech. Rep. CERC Field Research Facility, Vicksburg, Miss., 1988, p. 81.
22. Bowen, A. J. and Holman, R. A., *J. Geophys. Res.*, 1989, **94**(C12), 18023–18030.
23. Oltman-Shay, J., Howd, P. A. and Birkemeir, W. A., *J. Geophys. Res.*, 1989, **94**(C12), 18031–18042.
24. Putrevu, U. and Svendsen, Ib. A., *J. Geophys. Res.*, 1993, **98**(C12), 22707–22717.
25. Kim, C. S. and Huntley, D. A., *J. Geophys. Res.*, 1985, **91**(C3), 3967–3978.
26. Huntley, D. A., Simmonds, D. and Tatavarti, R., *Coastal Engg.*, 1995, (communicated).
27. Silvester, R., *Coastal Sediments '77*, 1977, pp. 639–654.
28. Kraus, N. C. and McDougal, W. G., *J. Coastal Res.*, 1994.
29. McDougal, W. G., Kraus, N. C. and Ajiwibowo, H., *J. Coastal Res.*, 1994.

ACKNOWLEDGEMENTS. This study was sponsored by SERC, DST, New Delhi under the project 'Sediment dynamics and hydrodynamics of mudbanks off Kerala' (ESS/CA/A1-14/93). Tatavarti thanks Director, NPOL for his encouragement. Dr K. R. Gupta, DST, is gratefully acknowledged for his encouragement and invaluable assistance. The project team gratefully acknowledge the logistic support and encouragement provided by Dr Shanmugam, Allepey and Shri Gopalakrishnan and family, Purakkad during the field experiments.

Received 18 October 1995; revised accepted 6 March 1996

Predominance of plate motion-related strain in the south Indian shield

D. S. Ramesh, R. N. Bharthur*, K. S. Prakasam, D. Srinagesh, S. S. Rai and V. K. Gaur†

National Geophysical Research Institute, Hyderabad 500 007, India
*GBA Seismic Array, BARC, Gauribidanur 561 208, India
†CMMACS, National Aerospace Laboratories, Belur Campus, Bangalore 560 037 India

Seismic anisotropy in the lithosphere, manifested by the splitting of shear waves into two orthogonal polarizations directions, is related to the lattice preferred orientation of olivine, which in turn is influenced by the direction of flow in the mantle[1,2]. Such anisotropy inferred beneath Precambrian terrains is interpreted as related to either present day plate motion (mantle flow direction)[3,4] or ancient anisotropy fossilized in Precambrian terrains[5]. We present here data from digital broadband seismographs at Hyderabad and Gauribidanur, which indicate that the azimuth of seismic anisotropy is closely aligned with the present day northward direction of absolute plate motion for India. These results confirm our earlier findings from analogue seismic data elsewhere[3] wherein we infer that shearing of the sublithospheric mantle by the moving plate results in resistive drag by the mantle leading to preferred crystallographic orientation near the base of the plate.

FLOW of the mantle beneath stable continental interiors is best documented by the observation of the phenomenon of shearwave splitting due to mantle anisotropy. Seismic anisotropy may be caused by the preferred orientation of anisotropic materials such as mantle minerals (mainly olivine, orthopyroxene), that tend to become aligned in the flow direction during rock deformation. Thus, the shear history and, therefore, the finite strain involved forge preferential orientations in material giving rise to the observed anisotropic seismic velocities in a particular direction. Laboratory experiments[6], theoretical modelling studies[1,2] and observations on natural anisotropic crystals[7] reveal that the fast polarization direction is parallel to the crystallographic axis [100]. This in turn is found to exhibit the same parallelism with the extension direction for nearly all types of finite strain that encompass the various tectonic processes. Therefore the fast polarization direction, strain-induced lattice deformation and orientation of finite strain principal axes have a definite relationship based on the nature of the tectonic process.

An established tool to study azimuthal anisotropy is to observe shearwave splitting in seismic phases, SKS and SKKS, which propagate through the Earth's core and arrive at the receiver in a near vertical direction. Their polarization is controlled almost exclusively by